Korean J. Chem. Eng., **28**(2), 402-408 (2011)
DOI: 10.1007/s11814-010-0356-7

Effects of La_2O_3 on ZrO_2 supported Ni catalysts for autothermal reforming of CH_4

Sun Hee Park, Byung-Hee Chun, and Sung Hyun Kim†

Department of Chemical and Biological Engineering, Korea University, Anam-dong, Seongbuk-gu, Seoul 136-701, Korea
(*Received 17 May 2010 • accepted 12 June 2010*)

Abstract−The effect of La_2O_3 content in Ni-La-Zr catalyst was investigated for the autothermal reforming (ATR) of CH_4. The catalysts were prepared by the coprecipitation method and had a mesoporous structure. Temperature programmed reduction (TPR) and X-ray photoelectron spectroscopy (XPS) indicated that a strong interaction developed between Ni species and the support with the addition of La_2O_3. Thermogravimetric analysis (TGA) and H_2-pulse chemisorption showed that the addition of La_2O_3 led to well dispersed NiO molecules on the support. Ni-La-Zr catalysts gave much higher CH_4 conversion than Ni-Zr catalyst. The Ni-La-Zr containing 3.2 wt% La_2O_3 showed the highest activity. The optimum conditions for maximal CH_4 conversion and H_2 yield were H_2O/CH_4=1.00, O_2/CH_4=0.75. Under these conditions, CH_4 conversion of 83% was achieved at 700 °C. In excess O_2 (O_2/CH_4>0.88), the catalytic activity was decreased due to sintering of the catalyst.

Key words: Methane, Reforming, Autothermal, Lanthanum, Zirconium Oxide, Nickel Catalyst

INTRODUCTION

Autothermal reforming (ATR) of CH_4 is a combination of steam reforming (SR) and partial oxidation (PO) of CH_4 [1-8]. SR is a highly endothermic reaction that requires an external heat source. On the other hand, PO is an exothermic reaction which can act as the internal heat supply for the SR reaction. Utilizing an internal heat supply is more energy efficient than using an external-heat source [9]. However, O_2 fed with CH_4 and H_2O results in hotspot formation, which leads to the sintering of catalyst. Coking is also a major problem in ATR; therefore, both sintering and coking are serious issues associated with catalysis in academic research and commercial industries.

Commercial industries typically use Ni as the active metal for reforming of CH_4, because it is cheaper than noble metals such as Pd, Rh, Ru and Pd. Many Ni-based catalysts are used for steam reforming of CH_4. In these systems, the supply of H_2O/CH_4 is high enough to decrease coking in the catalysts. However, these commercial catalysts are not suitable for ATR, because coking and sintering by the formation of hotspots from partial-oxidation reactions occur faster than steam reforming under excess steam of H_2O/CH_4> 2.5 below 700 °C.

The development of novel catalysts for reforming of CH_4 has primarily focused on keeping the catalytic activity from either forming hotspots or coking. Most of the catalysts developed in the previous researches performed well at temperatures of around 750 °C [1,10-12]. Only a few studies were able to demonstrate high catalytic activity at and below 700 °C, which decreases the performance of the catalysts significantly [13-15]. Therefore, our experiments were performed at 700 °C to maximize the catalytic activity.

This study chose ZrO_2 as the support, which typically displayed Lewis acid properties and high thermal stability [15-17]. The tetragonal phase of ZrO_2 enhances the thermal stability of the catalysts and allows them to endure the increased temperature at hotspots, which are approximately 100 °C higher than operating temperature of the system. We used La_2O_3 as an additive to lower coking in the catalysts, because La_2O_3 is known to limit the formation of coke. However, La_2O_3 can reduce the activity of the catalysts if the added amount is higher than the optimal level. Martinez et al. used a small amount of La_2O_3 in Ni-Al_2O_3 catalysts for CO_2 reforming of CH_4 [18]. The catalytic performance, such as conversion of CH_4 and H_2 yield, can be improved by changing a feed stream. The ratio of H_2O/CH_4 and O_2/CH_4 is an important parameter in ATR. Most of the studies for the steam reforming CH_4 use a syringe pump to provide the feed steam into the reactor. However, the syringe pump has disadvantages such as pulse injection, heterogeneous mixing of gases and steam and periodic refill of water in the syringe. We solved these problems by using a steam-supply system that was similar to a humidifier.

The goals of this study were to examine the influence of La_2O_3 on ZrO_2-supported Ni catalysts prepared by coprecipitation method and to increase the performance of the catalysts by adjusting the feed stream in ATR.

EXPERIMENTAL

1. Preparation of Catalysts

Ni-La-Zr catalysts containing different amounts of La_2O_3 were synthesized by the coprecipitation method. $Ni(NO_3)_2 \cdot 6H_2O$, $La(NO_3)_2 \cdot 6H_2O$ and $ZrO(NO_3)_2$ dissolved in the deionized water were used as the precursor solution and a solution of NH_4OH was used as the precipitating reagent. The precipitation was carried out at a constant temperature of 50 °C with continuous stirring of 500 rpm for 24 h. The precursor solution was dropped into a diluted solution of NH_4OH until the optimum pH was achieved. The optimum pH was determined to be 8.05, because this pH provided adequate La content with a low loss of Ni [11]. Variation range of pH during the

†To whom correspondence should be addressed.
E-mail: kimsh@korea.ac.kr

precipitation and aging was 7.95 to 8.15. The obtained precipitate was filtered, washed and dried at 110 °C for 24 h. This material was calcined at 750 °C for 4 h. It was then sieved and the particle size range was determined to be 75-150 μm. We synthesized four different catalysts containing 15.0 wt% NiO and different La_2O_3 concentrations of 0.0, 1.7, 3.2 and 6.8 wt%.

2. Methods of Characterization

Elemental analysis of calcined catalysts was performed by inductively coupled plasma atomic emission spectrophotometer (ICP-AES, 138 Ultrace, Jobin Yvon). XRD measurements of the calcined catalysts were performed by X-ray diffractometer (X'Pert MPD, Philips) with CuKα (λ=0.1538 nm) radiation. The XRD patterns were obtained in the 2θ range of 5-85 degree at a scan speed of 0.04°/s. and were identified by comparison with JCPDS database cards.

The textural properties of the calcined catalysts were determined by N_2 adsorption and desorption isotherms at −196 °C. The catalysts were pretreated at 300 °C for 5 h under vacuum of 10^{-4} mbar to create a clean surface. The specific areas of the catalysts were evaluated by the Brunauer, Emmett and Teller (BET) theory. The pore size distribution was calculated by the desorption branch of the isotherm based on the Barrett, Joyner and Halenda (BJH) method.

NiO dispersion was measured by H_2-pulse chemisorptions at 298 K with Ar flow of 50 ml/min and pulse of 10% H_2 in Ar of 0.1 ml by ASAP 2010. Catalysts were reduced under H_2/Ar flow of 50 ml/min for 1 h at 923 K and subsequently flushed under Ar for 15 min at 15 K. Adsorption stoichiometry of H/Ni=1 was assumed to calculate metal dispersion.

H_2-TPR profiles of the calcined catalysts were performed in a semiautomatic apparatus (BEL CAT-M, BEL Japan Inc.) equipped with a thermal conductivity detector (TCD). The 50 mg of fresh catalyst was placed in a quartz tube. The temperature was increased to 200 °C in a 20 mol% O_2/He mixture gas flow of 70 ml/min at heating rate of 10 °C /min and maintained at 200 °C for 1 h. The system was then cooled to room temperature. The TPR profile of the fresh catalyst was recorded in a 10 mol% H_2/Ar mixture gas flow of 30 ml/min while heating up to 800 °C at a heating rate of 8.2 °C/min. A moisture trap containing 10 g of molecular sieve 3A was placed just before the TCD with sensitivity of 50 mV.

XPS was used to determine the binding energy (BE) of Ni, which was the active metal. Photoelectron spectra were recorded with a monochromator Al Kα X-ray source (hv=1486.6 eV) and anode (250 W, 10 kV, 27 mA). The C 1s, Zr 3d, La 3d, and Ni 2p core-level spectra were recorded and the corresponding binding energies were calibrated by the C 1s line at 284.6 eV.

3. Catalytic Reaction

ATR of CH_4 was carried out under atmospheric pressure in a fixed bed quartz reactor (I.D.=4 mmØ, O.D.=6 mmØ, length=300 mm). An electronic furnace in the reactor was connected to a thermo-controller. 45 mg of the catalyst (GHSV=60,000 ml/h·g_{cat}) was fixed into the middle of the reactor with quartz wool. A thermocouple was inserted under quartz wool in the reactor to measure the bed temperature. Before the reaction was allowed to occur at 700 °C, the catalyst was reduced in 10% H_2/N_2 mixture gas flow of 100 ml/min at 700 °C for 1 h. After reduction, the feed gases, which were a mixture of CH_4, O_2, steam (H_2O) and N_2, were introduced into the catalyst bed. The amount of H_2O was calculated by Dalton's law of partial pressure, because the water was supplied by a humidifier not a micro-liquid pump. These conditions were satisfied at 58 °C (saturated vapor pressure: 18.15 kPa) at atmospheric pressure at an H_2O flow rate of 15 ml/min and a total flow rate of feed of 85 ml/min. We removed condensation from the steam through a line that was connected to the reactor by maintaining the temperature of the humidifier at 58 °C and the line around 65 °C. The ratio of feed was maintained at a constant value. CH_4, O_2 and N_2 were fed into the bottom of the humidifier with a mass flow controller (MFC), after which they were mixed. The humidifier was 150 mm in diameter and 500 mm in length. The partial pressure ratio of the feed gases was $CH_4 : H_2O : O_2 : N_2$=20 : 15 : 10 : 40. An iced water trap was placed before the gas chromatograph (GC) to remove the steam contained in the effluent gas. The effluent gas was analyzed by GC (HP7890, Agilent) with a thermal conductivity detector (TCD). A switching system containing a two-column valve was used. Concentrations of H_2, O_2, N_2, CH_4, CO were determined using a stainless steel column packed with a molecular sieve 5A, which could not separate CO_2. The concentration of CO_2 was determined by using a porapak Q column. CH_4 conversion and H_2 yield in ATR was determined as described below:

$$CH_4 \text{ conversion } (\%) = \text{moles of } CH_4 \text{ reacted/moles of } CH_4 \text{ fed} \times 100 \quad (1)$$

$$H_2 \text{ yield } (\%) = \text{moles of } H_2 \text{ formed}/(2 \times \text{moles of } CH_4 \text{ fed}) \times 100 \quad (2)$$

RESULTS AND DISCUSSION

1. Characterization of Catalysts

Fig. 1 shows the XRD patterns of the catalysts with different amounts of La_2O_3 after calcinations at 750 °C for 4 h. The ZrO_2 in the catalysts were in the crystalline tetragonal phase. Tetragonal phase was stabilized at room temperature without the addition of any dopants. This can be explained by the nano-size effect, which affects the crystalline phase composition [16]. Cell parameters a and c were 5.09 and 5.18, respectively, for the tetragonal ZrO_2 (JCPDS 140534). All the patterns of the tetragonal phase of ZrO_2 correspond to (1 1 1), (2 0 0), (2 2 0), (3 1 1) and (4 0 0) planes. The peak of La_2O_3 or

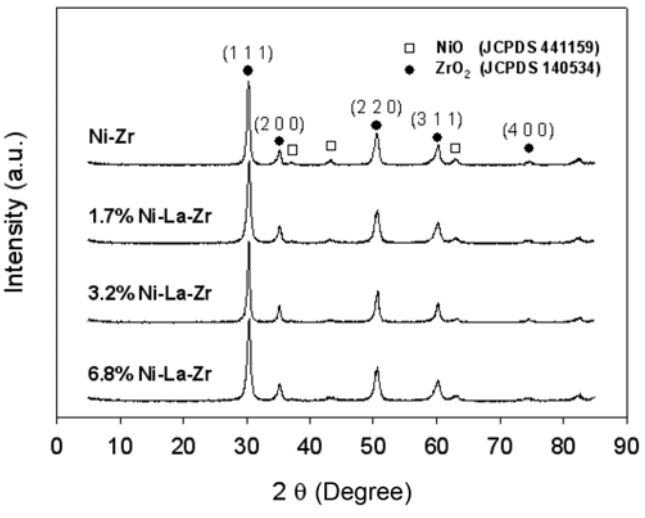

Fig. 1. XRD patterns of Ni-La-Zr calcined at 750 °C with different La_2O_3 concentrations.

Table 1. Chemical composition (wt%) of calcined catalysts

Catalyst	NiO	La_2O_3	ZrO_2
Ni-Zr	15.2	0.0	balance
1.7% Ni-La-Zr	14.9	1.7	balance
3.2% Ni-La-Zr	15.1	3.2	balance
6.8% Ni-La-Zr	15.2	6.8	balance

Table 2. Structural properties of calcined catalysts

Catalyst	Surface area (m^2/g)	Total pore volume (cm^3/g)	Mean pore diameter (nm)
Ni-Zr	43.44	0.046	6.69
1.7% Ni-La-Zr	42.77	0.045	6.70
3.2% Ni-La-Zr	43.84	0.047	6.65
6.8% Ni-La-Zr	42.74	0.048	6.66

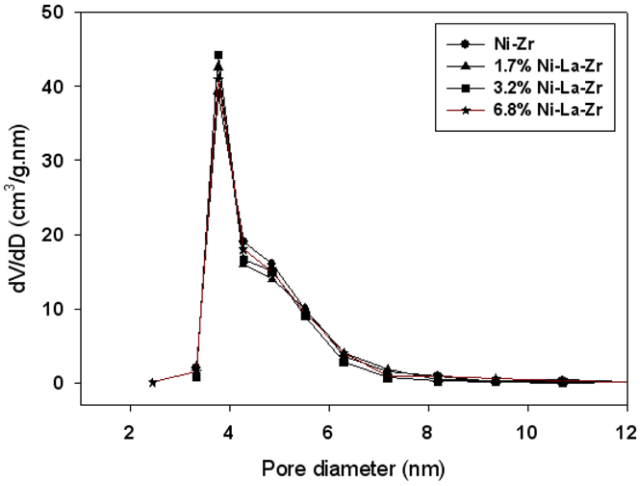

Fig. 2. Pore size distribution of catalysts determined from the BJH method.

solid solution containing La_2O_3 was not detected, because the amount of La_2O_3 was small and well dispersed.

Table 2 shows the important textural parameters evaluated from the N_2 adsorption and desorption isotherms such as the BET specific surface area, total pore volume and mean pore diameter. The pore size distributions of the catalysts are shown in Fig. 2. All catalysts possessed uniform pore size distributions. This result indicated that pore size of catalyst was not affected by the amount of La_2O_3. Isotherms of the catalysts are shown in Fig. 3. According to IUPAC, the shape of the catalyst isotherms was classified as a type IV isotherm, which represented the adsorption isotherm of a hysteresis loop and the characteristics of mesoporous adsorbents with strong affinity. The characteristic features of Type IV isotherm are its hysteresis loop, which is associated with capillary condensation taking place in mesopores, and the limited uptake at a high P/P_o.

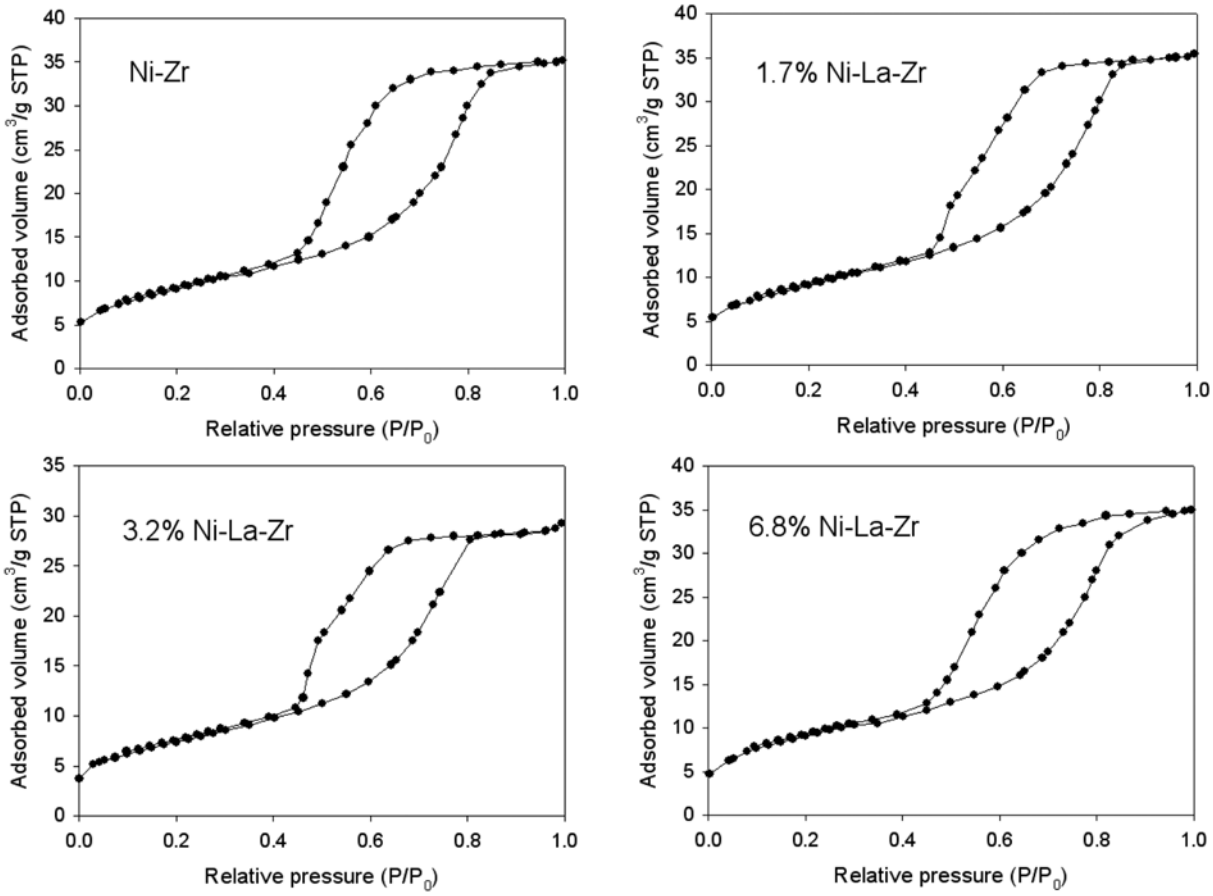

Fig. 3. N_2 adsorption and desorption isotherms of the catalysts.

Table 3. H_2 chemisorption results on calcined catalysts and used catalysts

Catalyst	Ni surface area (m^2/g_{Ni})		Ni size (nm)		Metal dispersion (%)	
	Calcined	Used	Calcined	Used	Calcined	Used
Ni-Zr	3.3	2.9	14.1	14.8	7.1	6.8
1.7% Ni-La-Zr	4.9	4.8	12.1	12.2	8.3	8.2
3.2% Ni-La-Zr	5.6	5.5	10.5	10.6	9.5	9.4
6.8% Ni-La-Zr	4.7	4.5	12.6	12.8	7.9	7.8

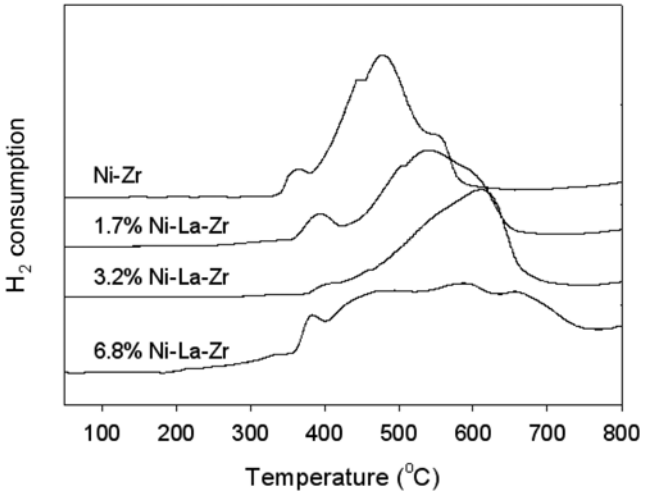

Fig. 4. TPR profiles of the catalysts.

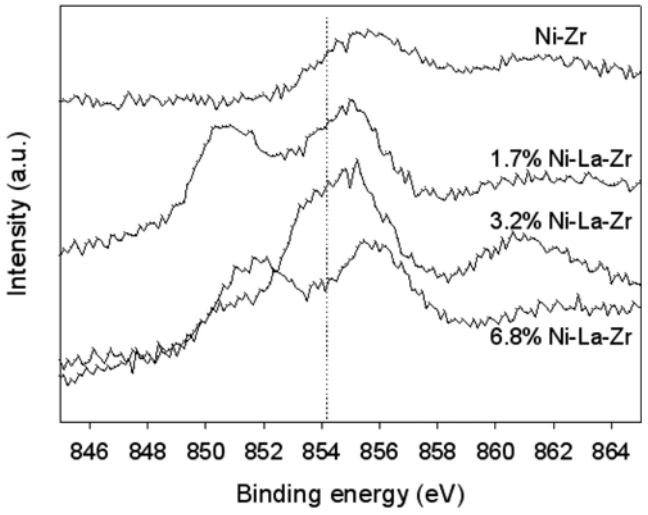

Fig. 5. XP spectra of the catalysts.

The initial region of the Type IV isotherm was attributed to monolayer-multilayer adsorption. It followed the same path as the corresponding region of a Type II isotherm obtained with the given adsorptive on the same surface area of the adsorbent in a nonporous form [19,20]. Correlation coefficients in the BET plot of all catalysts were 1. The C-value means heat of adsorption and usually 50-300 in the BET equation [21]. The C-value of all catalysts was above zero. The C-value above zero guarantees that the measured surface area is accurate. The interval of relative pressure ranged from 0.02 to approximately 0.3.

As indicated in Table 3 by H_2 chemisorption, the addition of La_2O_3 decreased the Ni crystallite size and led to increase Ni dispersion until the amount of it reached 3.2 wt%. The TPR profiles of the catalysts with various amounts of La_2O_3 are shown in Fig. 4. A peak assigned to the free NiO species, which have not interacted with the support, was first observed between 300 °C and 400 °C [12]. The peak initially observed at around 380 °C could be due to the reduction of bulk Ni, which has a low interaction with the support. The second peak at higher temperatures may be related to the reduction of Ni having stronger interactions with the support. The TPR profiles show that the interaction between Ni and the support become stronger when the amount of La_2O_3 was increased up to 3.2 wt%. The small peak observed at approximately 400 °C for the 3.2 wt% Ni-La-Zr catalyst indicated that NiO was well dispersed on the support and did not aggregate into bulk NiO. When the concentration of La_2O_3 was increased to 6.8 wt%, a peak at about 390 °C appeared. This result explained that the dispersion of NiO was poor when the La_2O_3 concentration was higher than 3.2 wt%. These TPR results corresponded to H_2 chemisorption results, that the highly dispersed NiO had relatively strong interaction with the support.

Fig. 5 shows the XPS spectra of Ni-La-Zr catalysts. The binding energy of free NiO has been reported to be 854.2 eV [22]. The BE for $Ni_{2p3/2}$ of all catalysts was above 854.2 eV and some were as high as 856.0 eV. This observation indicates that NiO_x species have strong interaction with the support and its strength is proportional to the amount of La_2O_3.

2. Reaction Results

2-1. Effect of Time on Stream

ATR of CH_4 was carried out over a Ni-La-Zr catalyst containing La_2O_3 in concentration range from 0 wt% to 6.8 wt% at 700 °C, GHSV =60,000 ml/h·g_{cat} and $CH_4 : H_2O : O_2 : N_2$=20 : 15 : 10 : 40 (H_2O/CH_4=0.75 and O_2/CH_4=0.5). Fig. 6 shows the CH_4 conversion and H_2 yield of the reactions. Both CH_4 conversion and H_2 yield increased as the La_2O_3 concentration was increased up to 3.2 wt% and decreased at 3.2 wt% above. This means that 3.2 wt% is the optimum La_2O_3 concentration for catalytic activity. The catalytic activity of all catalysts containing La_2O_3 remained constant without any significant decrease at the reaction time of 50 h above. On the other hand, the activity of Ni-ZrO_2 decreased after 24 h. These results were due to the thermal stability of the tetragonal phase of ZrO_2, the ability of La_2O_3 to suppress coke formation [15] and the strong interaction between NiO and the support. Coking formed on the catalyst was quantitatively measured by TGA. Fig. 7 shows TGA results of the used catalysts. The catalyst weight decreases due to the carbon gasification. Until about 300 °C, the initial weight loss is ascribed to the thermal desorption of H_2O and CO_2 and removal of easily oxidizable carbonaceous species. Above 500 °C, the weight

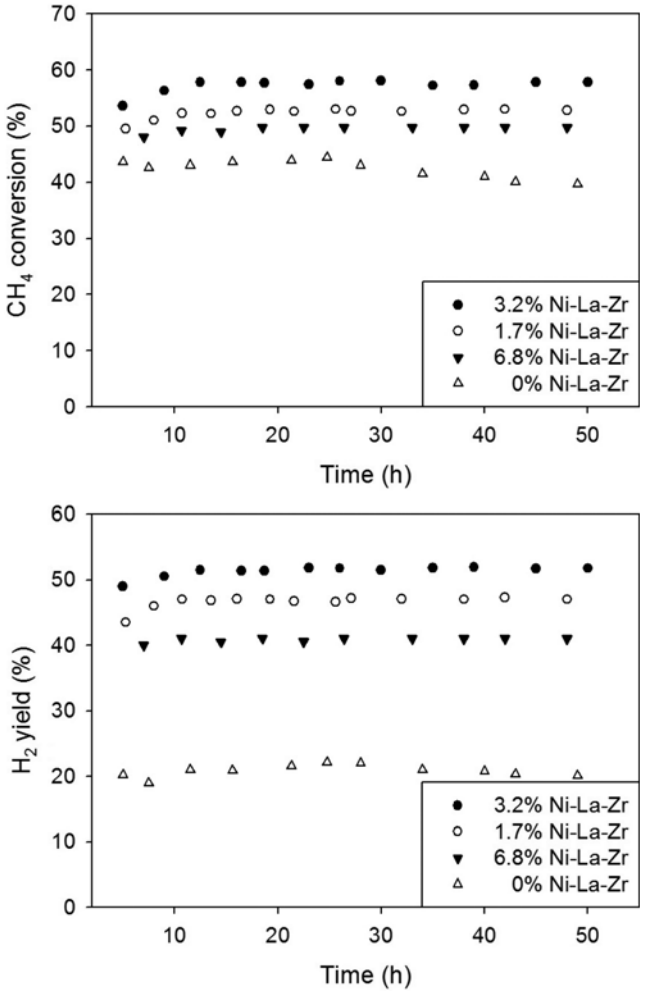

Fig. 6. CH_4 conversion and H_2 yield as a function of time over Ni-La-Zr catalysts containing different La_2O_3 concentrations (T=700 °C, GHSV=60,000 ml/h·g_{cat}, $CH_4 : H_2O : O_2 : N_2$= 20 : 15 : 10 : 40).

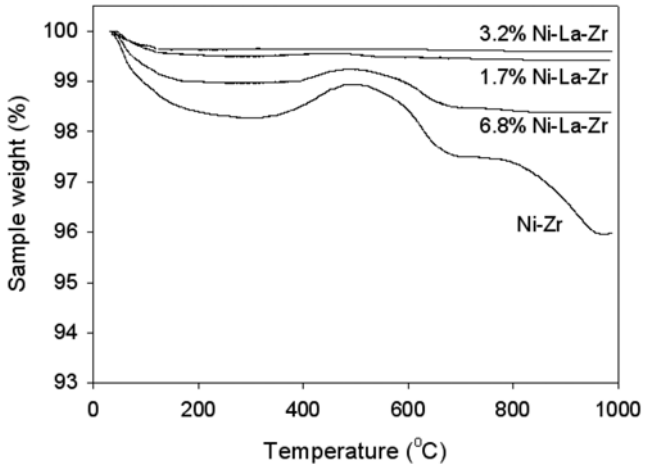

Fig. 7. TGA profiles of used catalysts under air.

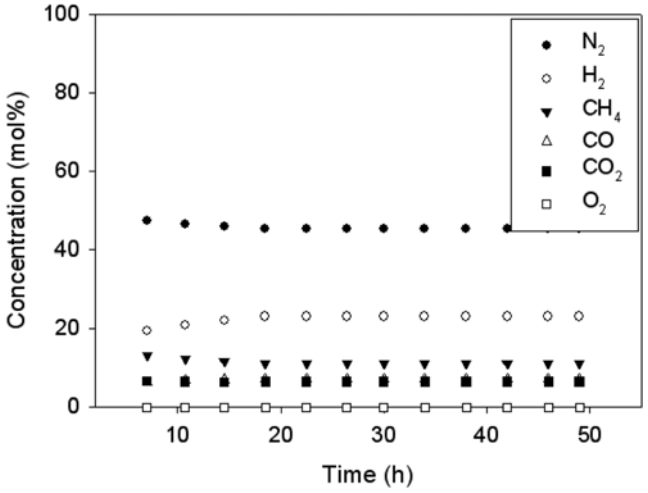

Fig. 8. Concentration of product gases over 1.7% Ni-La-Zr (T= 700 °C, GHSV=60,000 ml/h·g_{cat}, $CH_4 : H_2O : O_2 : N_2$=20 : 15 : 10 : 40).

decrease is due to the oxidation of coke to CO and CO_x. Between 400 and 450 °C, the increase of weight occurs by the oxidation of Ni particles[14]. Weight of both Ni-Zr (0.0 wt% Ni-La-Zr) and 6.8 wt% Ni-La-Zr increases in this temperature interval, while 1.7 wt% and 3.2 wt% Ni-La-Zr do not show change of their weight. This result can be explained that the addition of La_2O_3 improves the dispersion of Ni, which results in the strong interaction with support. These highly dispersed Ni particles are hard to oxidize. These results correspond to H_2-TPR profiles in which reduction of catalysts with La_2O_3 is difficult. Table 3 shows that NiO dispersion in the used catalysts including La_2O_3 after reaction barely decreased before reaction. La_2O_3 promoted interaction NiO and support to prevent NiO dispersion from being deteriorated.

The deposition of carbon during CH_4 reforming would occur from the decomposition of CH_4 or CO disproportionation, which is thermodynamically favorable below 900 °C [23,24]. Formation of coke is related to the acidity of the catalyst. ZrO_2 used as a support possesses both acidic and basic properties [13]. Acids and bases are neutralized in solutions, but they exist independently on the surface. These acid-base bifunctional properties of ZrO_2 are suitable not only for the activity of the catalyst but also for the formation of coking. The basic property of La_2O_3 reduces the acidity of the catalyst, lowering coking on the surface of the catalyst [13,14,25] and can make filamentous carbon, which plugs pores and reduces cracking of the catalyst [11,15]. Because the decrease in acidity of the catalyst can make unstable carbide, carbonaceous species from CH_4 and CO are active and can easily leave the surface of the catalyst through the formation of CO_2 to improve CH_4 conversion. However, when the amount of La_2O_3 was higher than the optimum concentration, there was poor dispersion of La_2O_3 and a decrease in the acidity of catalyst [11].

2-2. Effect of Feed Ratio

The efficiency of the ATR reaction is affected not only by the activity of the catalyst but also by the operating conditions such as the ratio of feed gases. The catalyst containing 1.7 wt% La_2O_3 was selected to examine the effects of different feed gas ratios on both the CH_4 conversion and H_2 yield under constant reaction conditions (T=700 °C, GHSV=60,000 ml/h·g_{cat}). As shown in Fig. 8, the composition of O_2 in the product gases was 0% at O_2/CH_4=0.5 while

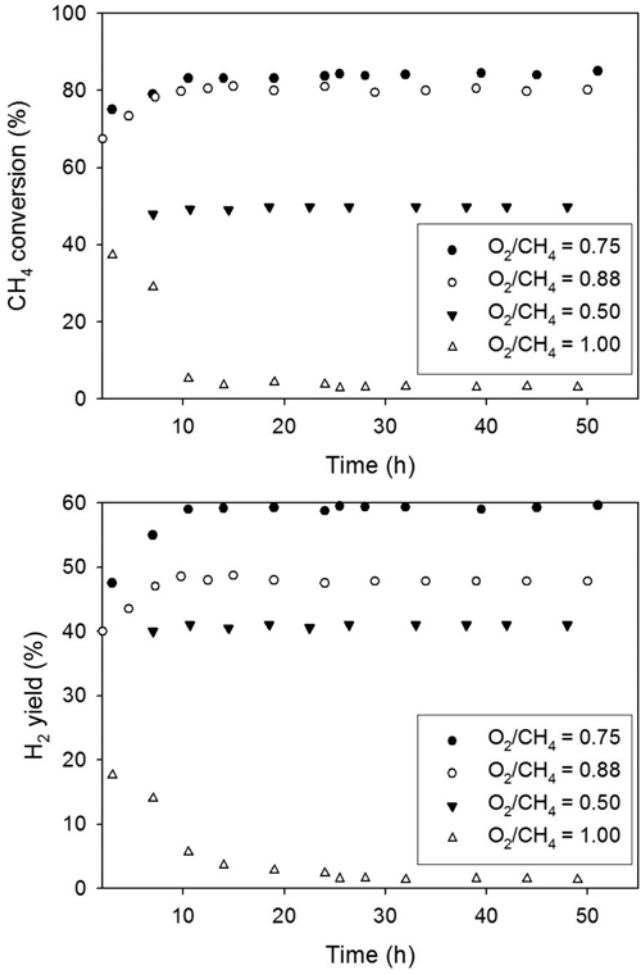

Fig. 9. CH_4 conversion and H_2 yield at different O_2/CH_4 ratios over 1.7% Ni-La-Zr (T=700 °C, GHSV=60,000 ml/h·g_{cat}).

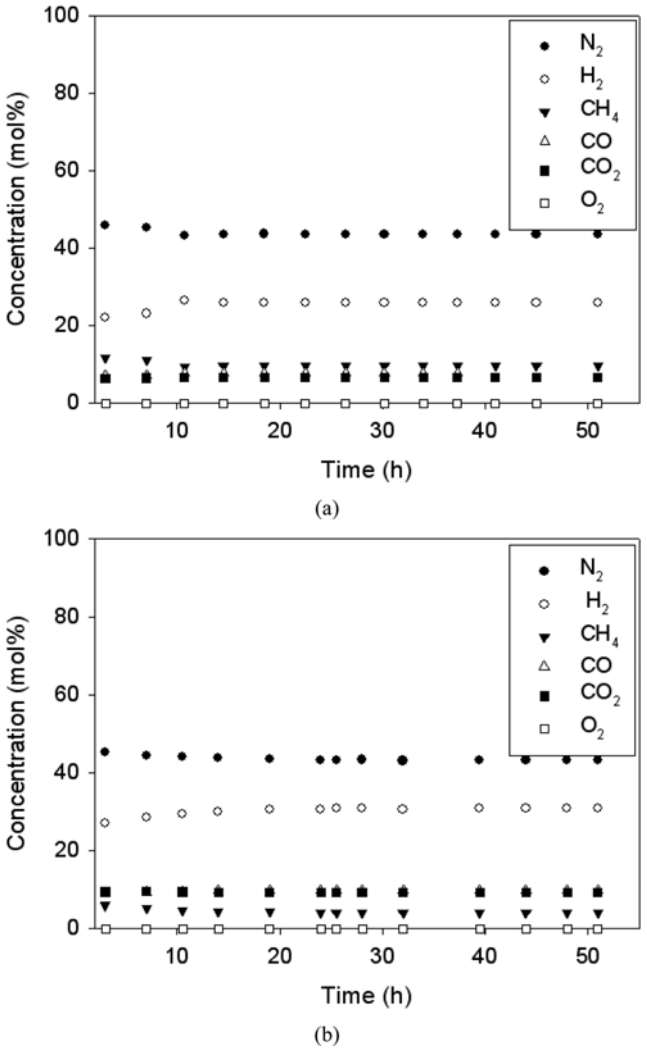

Fig. 10. Concentration of product gases over 1.7% Ni-La-Zr at (a) O_2/CH_4=0.50 and (b) O_2/CH_4=0.75 (T=700 °C, GHSV= 60,000 ml/h·g_{cat}).

CH_4 was detected by TCD and some water condensed in the iced water trap following the reactor. Four different O_2/CH_4 ratios (0.5, 0.75, 0.88 and 1.00) were examined. The CH_4 conversion (O_2/CH_4= 0.75) increased by 25% and reached 88% relative to that at O_2/CH_4= 0.50 (Fig. 9). The H_2 yield also improved by over 15% compared to that at O_2/CH_4=0.50. At an O_2/CH_4 ratio of 0.88, the CH_4 conversion did not change and the H_2 yield decreased to 46% at a reaction time of 24 h. These results could be explained by the fact that the combustion of CH_4 was not used for PO at an excess of O_2 (O_2/CH_4>0.88). When the ratio of O_2/CH_4 was increased to 1.00, both CH_4 conversion and H_2 yield decreased immediately after the start of the reaction and reached approximately 0% after 10 h. These results demonstrate that the optimum ratio of O_2/CH_4 was around 0.75 for the operation of ATR.

The mechanism of PO, which is relatively faster than SR on the catalyst, is followed by the pyrolytic process and CO is formed but CO_2 is not. This mechanism has two steps: pyrolysis ($CH_4 \rightarrow C+4H$) occurs first and CO is formed from the oxidation of carbon in the second step [10,26]. Based on the proposed mechanism, CH_4 and O_2 could be dissociated on Ni site. La^{3+}, which is the reduced form of La_2O_3 and can increase the dispersion of metallic Ni [11], improves dissociation of CH_4 to lower the amount of coking accumulated in the active metal or interface of the support and active metal by decreasing the acidity of the catalyst. The general mechanism of SR through the dissociated adsorption of methane on the catalyst surface is shown by Dong [10] and Trimm [27]. H_2O can adsorb on either Ni sites or the support, while dissociation of CH_4 occurs on the active Ni sites. The support plays a direct a role in the reforming reaction. ZrO_2, as a Lewis acid, provides an active site for H_2O and enhances the mobility of OH to thermally stabilize the catalyst. Therefore, the surface of the catalyst is covered with C, CH_x, O and OH after dissociation of CH_4 from the Ni sites and dissociative adsorption of H_2O and O_2. The coverage of O species from dissociative adsorption of O_2 is much higher than that of O and OH species from dissociative adsorption of H_2O, because the dissociative adsorption of O_2 is much easier than H_2O on both the Ni and support of ATR [10]. As a result, the C, which is an intermediate in the dissociation of CH_4, may react with O species, which result from the dissociative adsorption of O_2. This proposed mechanism is outlined in Fig. 10. Fig. 10 shows that O_2 was completely consumed in the reaction at both O_2/CH_4=0.50 and 0.75. It is reason-

able that addition of O_2 into the feed improves either CH_4 conversion or H_2 yield before excess O_2 (O_2/CH_4>0.88) sinters the catalyst (Fig. 9).

CONCLUSIONS

Autothermal reforming of CH_4 was investigated for Ni-La-Zr catalysts prepared by coprecipitation. The coprecipitated Ni-La-Zr catalysts had a mesoporous structure and the ZrO_2 was in a crystalline tetragonal phase. TPR and XPS indicated that NiO species had strong interactions with the support and the strength of this interaction was proportional to the amount of La_2O_3. Catalysts containing 3.2 wt% La_2O_3 had the highest CH_4 conversion and H_2 yield and their activity remained constant during the entire reaction time. When the amount of La_2O_3 was increased to 6.8 wt%, the catalytic activity was lower than 3.2 wt%. Both CH_4 conversion and H_2 yield were enhanced at the optimum O_2/CH_4 ratio. However, an excess O_2 caused the catalyst to sinter and resulted in a deterioration of catalyst activity.

REFERENCES

1. X. Cai, X. Dong and W. Lin, *J. Nat. Gas Chem.*, **15**, 122 (2006).
2. S. Choi, I. Ahn and S. Moon, *Korean J. Chem. Eng.*, **26**, 1252 (2009).
3. J. C. Escritori, S. C. Dantas, R. R. Soares and C. E. Hori, *Catal. Commun.*, **10**, 1090 (2009).
4. J. Jun, K. Jeong, T.-J. Lee, S. Kong, T. Lim, S.-W. Nam, S.-A. Hong and K. Yoon, *Korean J. Chem. Eng.*, **21**, 140 (2004).
5. K. Koo, J. Yoon, C. Lee and H. Joo, *Korean J. Chem. Eng.*, **25**, 1054 (2008).
6. S. Park, K. Chun, W. Yoon and S. Kim, *Res. Chem. Intermed.*, **34**, 781 (2008).
7. H.-S. Roh and K.-W. Jun, *Catal. Surv. Asia*, **12**, 239 (2008).
8. H. M. Wang, *J. Power Sources*, **177**, 506 (2008).
9. Y. Mukainakano, B. Li, S. Kado, T. Miyazawa, K. Okumura, T. Miyao, S. Naito, K. Kunimori and K. Tomishige, *Appl. Catal., A*, **318**, 252 (2007).
10. W. S. Dong, *Catal. Lett.*, **78**, 215 (2002).
11. R. Martiez, E. Romero, C. Guimon and R. Bilbao, *Appl. Catal., A*, **274**, 139 (2004).
12. H.-S. Roh, K.-W. Jun, W.-S. Dong, J.-S. Chang, S.-E. Park and Y.-I. Joe, *J. Mol. Catal. A: Chem.*, **18**, 137 (2002).
13. K. Y. Koo, H.-S. Roh, Y. T. Seo, D. J. Seo, W. L. Yoon and S. Bin Park, *Int. J. Hydrogen Energy*, **33**, 2036 (2008).
14. K. Y. Koo, H.-S. Roh, Y. T. Seo, D. J. Seo, W. L. Yoon and S. B. Park, *Appl. Catal., A*, **340**, 183 (2008).
15. M. Rezaei, S. M. Alavi, S. Sahebdelfar, P. Bai, X. M. Liu and Z. F. Yan, *Appl. Catal., B*, **77**, 346 (2008).
16. T. Ma, Y. Huang, J. Yang, J. He and L. Zhao, *Mater. Des.*, **25**, 515 (2004).
17. K. T. Park, U. H. Jung, D. W. Choi, K. Chun, H. M. Lee and S. H. Kim, *J. Power Sources*, **177**, 247 (2008).
18. J.-M. Wei, B.-Q. Xu, J.-L. Li, Z.-X. Cheng and Q.-M. Zhu, *J. Mol. Catal. A: Chem.*, **196**, 167 (2000).
19. J. Rouquerol, *Pure Appl. Chem.*, **66**, 1739 (1994).
20. K. S. W. Sing, *Pure Appl. Chem.*, **57**, 603 (1985).
21. S. Brunauer, P. H. Emmett and E. Teller, *J. Am. Chem. Soc.*, **60**, 309 (1938).
22. A. Slagtern, Y. Schuurman, C. Leclercq, X. Verykios and C. Mirodatos, *J. Catal.*, **172**, 118 (1997).
23. A. M. Gadalla and B. Bower, *Chem. Eng. Sci.*, **43**, 3049 (1988).
24. S. C. Tsang, J. B. Claridge and M. L. H. Green, *Catal. Today*, **23**, 3 (1995).
25. M. C. Saìnchez-Saìnchez, *Int. J. Hydrogen Energy*, **32**, 1462 (2007).
26. D. A. Hickman, *Science*, **259**, 343 (1993).
27. D. L. Trimm, *Catal. Today*, **49**, 3 (1999).